Biophysical Journal
Article

Biophysical Society

Numerical simulation of flow characteristics in a permeable liver sinusoid with leukocytes

Shenbao Chen,[1,2] Jingchen Zhu,[1,2] Jian Xue,[2,3] Xiaolong Wang,[4] Peng Jing,[4] Lüwen Zhou,[1,2] Yuhong Cui,[5] Tianhao Wang,[5] Xiaobo Gong,[4,*] Shouqin Lü,[1,2,*] and Mian Long[1,2,*]

[1]Center of Biomechanics and Bioengineering, Key Laboratory of Microgravity (National Microgravity Laboratory), Beijing Key Laboratory of Engineered Construction and Mechanobiology, and CAS Center for Excellence in Complex System Mechanics, Institute of Mechanics, Chinese Academy of Sciences, Beijing, China; [2]School of Engineering Science, University of Chinese Academy of Sciences, Beijing, China; [3]State Key Laboratory of Nonlinear Mechanics (LNM), Institute of Mechanics, Chinese Academy of Sciences, Beijing, China; [4]Key Laboratory of Hydrodynamics (Ministry of Education), Department of Engineering Mechanics, School of Naval Architecture, Ocean and Civil Engineering, Shanghai Jiao Tong University, Shanghai, China; and [5]Department of Mechanics, Tianjin University, Tianjin, China

ABSTRACT Double-layered channels of sinusoid lumen and Disse space separated by fenestrated liver sinusoidal endothelial cells (LSECs) endow the unique mechanical environment of the liver sinusoid network, which further guarantees its biological function. It is also known that this mechanical environment changes dramatically under liver fibrosis and cirrhosis, including the reduced plasma penetration and metabolite exchange between the two flow channels and the reduced Disse space deformability. The squeezing of leukocytes through narrow sinusoid lumen also affects the mechanical environment of liver sinusoid. To date, the detailed flow-field profile of liver sinusoid is still far from clear due to experimental limitations. It also remains elusive whether and how the varied physical properties of the pathological liver sinusoid regulate the fluid flow characteristics. Here a numerical model based on the immersed boundary method was established, and the effects of Disse space and leukocyte elasticities, endothelium permeability, and sinusoidal stenosis degree on fluid flow as well as leukocyte trafficking were specified upon a mimic liver sinusoid structure. Results showed that endothelium permeability dominantly controlled the plasma penetration velocity across the endothelium, whereas leukocyte squeezing promoted local penetration and significantly regulated wall shear stress on hepatocytes, which was strongly related to the Disse space and leukocyte deformability. Permeability and elasticity cooperatively regulated the process of leukocytes trafficking through the liver sinusoid, especially for stiffer leukocytes. This study will offer new insights into deeper understanding of the elaborate mechanical features of liver sinusoid and corresponding biological function.

SIGNIFICANCE The specialized liver sinusoid microcirculation network, presenting a double-layered flow configuration of Disse space and sinusoidal lumen and the fluid penetration between the two channels via those fenestrae in LSECs, plays a key role for liver homeostasis. Structural complexity and technical limitations hinder the direct quantification of flow field of sinusoidal microcirculation, especially for the flow features in Disse space. This study performed numerical modeling based on the immersed boundary method to elaborate the effects of Disse space and leukocyte elasticities, endothelium permeability, and sinusoidal stenosis degree on sinusoidal flow field, which are evidently critical in elucidating the mass transportation mechanism of Disse space and the effect of flow on hepatocyte functions.

INTRODUCTION

The liver plays important roles in synthesis and metabolism of carbohydrate, protein, and lipid and detoxification as well as immune response. Inside an elementary unit of hepatic lobule, blood from both hepatic artery and portal vein are gradually mixed in the portal area, pass through the liver sinusoids, and finally drain into the central vein (1) (also refer to Fig. 1 *A*, upper panels). The portal vein system is formed by the confluence of splenic vein and superior mesenteric vein. Liver sinusoids, mainly composed of four kinds of cells—hepatocytes (HCs), liver sinusoidal endothelial cells (LSECs), hepatic stellate cells (HSCs), and Kupffer cells (KCs)—form a specialized capillary network for blood perfusion in the liver (1). The specificity of liver sinusoids

Submitted March 23, 2022, and accepted for publication October 17, 2022.

*Correspondence: x.gong@sjtu.edu.cn or lsq@imech.ac.cn or mlong@imech.ac.cn

Editor: Jing Chen.

https://doi.org/10.1016/j.bpj.2022.10.022

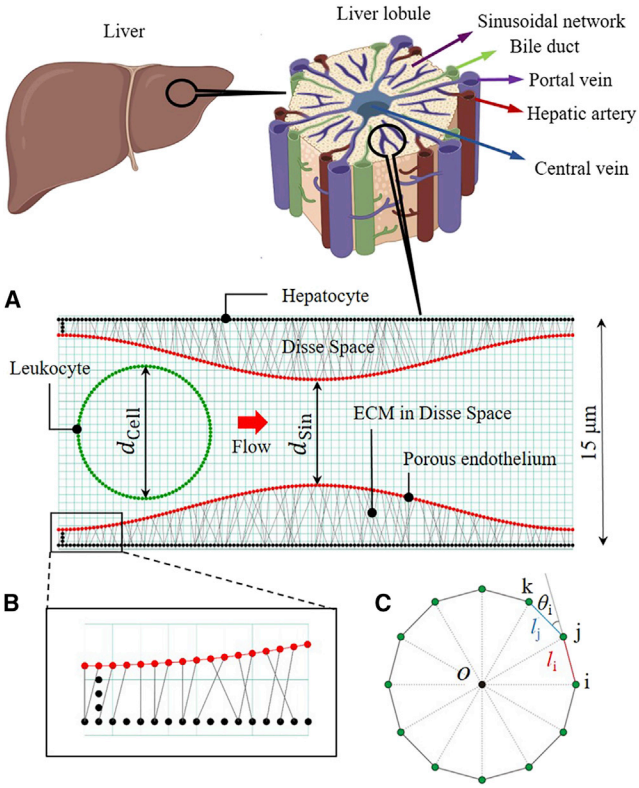

FIGURE 1 Numerical modeling of a leukocyte-presenting liver sinusoid using 2D IBM. (*A*) Schematic of the left one-third of the simulated liver sinusoid with sinusoidally varied lumen diameter d_{sin}. Background light green mesh grids represent the flow field. Dots of black, red, and dark green represent the hepatocyte layer, the liver endothelium, and the leukocyte, respectively. Gray lines connecting the hepatocyte layer and the endothelium denote the springs used to regulate the stiffness of Disse space. Also illustrated in the top two panels are the anatomic locations of liver sinusoids in both liver and liver lobule. (*B*) Zoomed view of one end of Disse space depicted as the black box in (*A*). Ends of Disse space are assumed to be closed (the right end is not plotted out for simplicity). Each node of endothelium is linked to one of the nearest four nodes in the hepatocyte layer. (*C*) Nodes and springs of the modeled leukocyte. Each node of the leukocyte is linked to the two neighboring nodes with an elastic spring. To see this figure in color, go online.

is embodied in their unique double-layer flow configuration constituted by both sinusoid lumen of 7–15 μm diameter and thin Disse space gap of 1–2 μm thickness. The former is surround by endothelium composed of LSECs and interspersed KCs; the latter separates the endothelium and the plate-like parenchymal HCs, and HSCs locate in the Disse space. Moreover, the fenestrae distributed through the LSECs, the weak junction between LSECs, as well as the lack of basement membrane under the endothelium allow mutual penetration between the sinusoidal lumen and the Disse space (1,2).

Liver sinusoid capillary network endows the liver with the most complicated microcirculation in human organs (3,4). Blood flow is one of key mechanical factors for liver functions. On the one hand, blood penetration through the sinusoidal endothelium exchanges the fluids inside the Disse space and in the sinusoidal lumen, and this fluid exchange guarantees the efficient supply of nutrients and oxygen to, and the effective taking of metabolic wastes away from, the hepatocyte layer. On the other hand, blood flow generates shear stress not only on the sinusoidal endothelium but also on the hepatocyte layer through the fluid penetration, regulating their functions cooperatively (5,6). However, it is still unclear how both the luminal flow in the sinusoidal main stream and the interstitial flow in the Disse space behave because of technical difficulties in quantifying these flows. In addition, the mechanical environment of liver sinusoid is dynamically altered in many physiological and pathological processes. Under pathological conditions such as liver fibrosis or cirrhosis, the defenestration (reduction or disappearance of fenestrae) of LSECs attenuates the permeability of the sinusoidal endothelium and reduces the interstitial flow inside the Disse space (7). Excessive deposition of extracellular matrices secreted by activated HSCs in the Disse space leads to significant changes in sinusoidal topography and reduces the deformability of the Disse space (8). Again, it is still unknown whether and how the alterations in sinusoidal mechanical properties influence the sinusoidal hemodynamics, especially at micro-flow scale.

Immune functions of the liver are also important for host immunity and survival (9–11), since a large number of external antigens from the digestive system enter into the liver through the portal vein and the liver is continuously exposed to an environment rich in blood-borne antigens. In this regard, circulating leukocytes play key roles for liver immune function by clearing external antigens. Effective recruitment of leukocytes in the liver is the prerequisite for their immunological function. In the process of liver inflammation, most leukocytes tend to recruit in liver sinusoids other than post capillaries, probably due to cooperative contributions of local structural and mechanical features of liver sinusoids as well as unique adhesion molecule expressions (12). For example, dynamic features of the flow indicated above drive leukocyte trafficking in the liver sinusoids, but the narrowness of the sinusoidal lumen constrains the leukocytes to deform and squeeze through (12,13). Experiments demonstrate that circulating leukocytes alter their deformability under chemical stimulations (14,15), which in turn affects cell trafficking in the sinusoids. However, how a leukocyte travels through liver sinusoid and how this process influences blood flow, fluid penetration, and wall shear stress (WSS) on hepatocytes in liver sinusoid are crucial issues for hepatic immune responses, which remain not fully understood.

Direct measurement of detailed fluid flow features in liver sinusoids in vivo is impracticable due to technical limitations. Liver on chip, an important technique in elucidating hepatic immune mechanism, is unsuitable to demonstrate the flow microenvironment of liver sinusoid because it is still technically difficult to fully reproduce the structure and physical or mechanical microenvironment of the liver

sinusoid in vivo. Thus, we proposed here a numerical model of the liver sinusoid when a leukocyte is squeezed through by shear flow. Based on the immersed boundary method (IBM) (16), we investigated the contributions of the elasticities of both leukocyte and Disse space, the permeability of sinusoidal endothelium resulting from the fenestrae in LSECs, and the stenosis alterations due to endothelium swelling in liver pathology to the dynamics features of blood flow and WSS endured by hepatocytes. Distributions of flow velocity, pressure, and WSS were specifically explored under varied conditions that mimic normal, fibrotic, or cirrhotic liver sinusoids.

METHODS

Theoretical modeling

To investigate the flow dynamics features in liver sinusoid, a two-dimensional (2D) micro channel with similar geometric characteristics both in height and the sinusoidal boundary with elasticity mimicking a real liver sinusoid was built (Fig. 1 *A*, lower panel, only one third of x direction with length of 100 μm from the inlet is shown for clarity), including fixed hepatocyte layer (dark nodes), deformable endothelium layer (red nodes), and a series of virtual springs connecting the hepatocyte layer and the endothelium functional as the intercellular matrix for regulating the stiffness of Disse space. Each node of the endothelium connected to its two neighboring endothelial nodes and to one of the nearest nodes of the hepatocyte layer simultaneously (Fig. 1 *B*). Sinusoidal lumen diameter was set sinusoidally varied along the flow direction. Nodes of the hepatocyte layer were fixed by hard springs connecting to fixed virtual nodes with the force defined as $f_{\text{fix}} = k_{\text{fix}} \cdot d_{\text{shift}}$, where k_{fix} was the spring constant and d_{shift} was the distance of a node deviating from its stress-free position. Deformation forces on springs connecting endothelium nodes and hepatocyte layer were defined as $f_{Diss} = k_{Diss}(l_i - l_{i0})$, where k_{Diss} was the spring constant, and l_i and l_{i0} were the instantaneous and resting lengths of the spring, respectively.

A leukocyte, modeled as a 2D capsule with viscous liquid inside enveloped by an elastic membrane representing the plasma membrane and the underlying cortex, was also introduced into the model for investigating its effect on flow features in the liver sinusoid. The cell membrane was discretized into N pieces of elastic segments connected at N evenly distributed nodes in which each node was linked to its neighboring nodes of both sides (Fig. 1 *A* and *C*). Strain energy for the leukocyte is composed of three components: stretching energy U_s (Eq. 1), bending energy U_b (Eq. 2), and area constrain energy U_A (Eq. 3) (17). Deformation forces on each node are calculated by taking the first derivative of strain energy with respect to node position. Strain energy and corresponding forces on endothelium nodes are defined in the same way as for the leukocyte but without the area conservation constraint.

$$U_s = \frac{1}{2}\Sigma_{i=1}^{N} k_s (l_i - l_0)^2 \tag{1}$$

$$U_b = \frac{1}{2}\Sigma_{i=1}^{N} k_b \tan^2\left(\frac{\theta_i - \theta_0}{\theta_0}\right)^2 \tag{2}$$

$$U_A = \frac{1}{2} k_A \left(\frac{A - A_0}{A_0}\right)^2 \tag{3}$$

where k_s, k_b and k_A are the elastic constants of virtual springs for stretching, bending, and area constrain energy of leukocyte, respectively. l_i, θ_i, and A are the instantaneous length, angle, and area of leukocyte, and l_0, θ_0, and A_0 are corresponding resting values (Fig. 1 *C*).

The leukocyte and the liver sinusoid were settled into a rectangular flow field with uniform density and viscosity of the blood plasma (Fig. 1 *A*, lower panel, green mesh grid). Initially, the fluid was static and the leukocyte was located at the left inlet of the channel. A uniform force density f_{dri} as local pressure difference was applied to each finite volume of fluid to generate a flow from the left to the right. The leukocyte was then enforced to flow with the fluid and deformed to squeeze through the liver sinusoid. To avoid nonphysical penetration between the leukocyte membrane and the endothelium layer, mirrored conditions with equivalent reversal repulsive forces were applied to those nodes on both sides when they got sufficiently close, with the force magnitude inversely proportional to distance as shown in Eq. 4, where k_{rep} is the spring constant of repulsive force, and d and d_{rep} are respectively the instantaneous distance and the defined lower limit distance between leukocyte and endothelium nodes,

$$f_{\text{rep}} = k_{\text{rep}}(d - d_{\text{rep}})/d_{\text{rep}}. \tag{4}$$

Numerical simulation

The IBM has been widely used to study fluid-cell interactions in blood cells circulation and cell bubble formation (18–21). Here the simulation framework was constructed based on the IBM and modified from an open-source package of MATLAB codes developed by Battista et al. (22,23), which was distributed on the Web site http://www.github.com/nickabattista/IB2d. All simulations were performed on the MATLAB platform. 2D Eulerian grid and one-dimensional (1D) Lagrangian grid were used to discretize the fluid domain and the immersed deformable boundaries, respectively. Hepatocytes layers were treated as rigid wall (black dots in Fig. 1 *A* and *B*), whereas the endothelial layers and the leukocyte were both elastic, represented by beams and springs (red and green dots in Fig. 1, respectively). In addition, the porous endothelial layers were endowed with permeability based on Darcy's Law and Peskin's method (24). Here the fluid velocity through a porous boundary is proportional to the pressure gradient between the two sides of this boundary and given by Eq. 5

$$U_p = -\frac{\kappa[p]}{\mu h} = -\frac{\kappa}{\mu h}\cdot\frac{\boldsymbol{F}\cdot\mathbf{n}}{||\boldsymbol{X}_s||}, \tag{5}$$

where U_p is the normal slip velocity through the porous endothelium, μ is the fluid viscosity, κ is the permeability coefficient, h is the thickness of the endothelium layer, $[p]$ is the pressure gradient across the layer, $\boldsymbol{F}$ is the constrain force density on endothelial nodes, $\boldsymbol{n}$ is a unit vector normal to the endothelium, and $\boldsymbol{X}_s$ is the differentiation of the membrane coordinates $\boldsymbol{X}(s, t)$ in curvilinear systems as $\partial\boldsymbol{X}(s, t)/\partial s$. Governing equations of the momentum conservation (Eq. 6) and continuity (Eq. 7) are expressed as the following:

$$\rho\left(\frac{\partial \boldsymbol{u}(\boldsymbol{x},t)}{\partial t} + \boldsymbol{u}(\boldsymbol{x},t)\cdot\nabla\boldsymbol{u}(\boldsymbol{x},t)\right) = -\nabla p(\boldsymbol{x},t) + \mu\Delta\boldsymbol{u}(\boldsymbol{x},t) + \boldsymbol{f}(\boldsymbol{x},t) \tag{6}$$

$$\nabla\cdot\boldsymbol{u}(\boldsymbol{x},t) = 0. \tag{7}$$

Here ρ, $\boldsymbol{u}(x, t)$, and $p(x, t)$ are the fluid density, fluid velocity, and pressure, respectively, and $\boldsymbol{f}(x, t)$ is the force density (force per unit area) performed to the fluid by deformed immersed boundaries. The independent variables are the position $\boldsymbol{x} = (x, y)$ and the time t. Numerical calculations were performed and iterated on four functional modules, including calculating the stress $\boldsymbol{F}(s, t)$ on an immersed boundary node, dispersing $\boldsymbol{F}$ to the neighboring fluid region (Eq. 8), updating the fluid velocity $\boldsymbol{u}$ (Eqs. 6 and 7)

and then the node velocity $\boldsymbol{U}$ (Eq. 9). Regularized Delta Kernel function in the cosine form was used for implementing force distribution and velocity interpolation (Eqs. 10 and 11). More details can be found in our previous work (25).

$$\boldsymbol{f}(\boldsymbol{x},t) = \int_{\Gamma} \boldsymbol{F}(s,t)\delta(\boldsymbol{x} - \boldsymbol{X}(s,t))\mathrm{d}s\ , \tag{8}$$

$$\boldsymbol{U}(\boldsymbol{X}(s,t),t) = -U_p\widehat{\boldsymbol{n}} + \int_{A} \boldsymbol{u}(\boldsymbol{x},t)\delta(\boldsymbol{x} - \boldsymbol{X}(s,t))\mathrm{d}\boldsymbol{x}, \tag{9}$$

$$\Phi(r) = \begin{cases} \frac{1}{4}\left(1+\cos\left(\frac{\pi r}{2}\right)\right) & |r| \le 2 \\ 0 & |r| > 2 \end{cases}, \text{and} \tag{10}$$

$$\delta_h(\boldsymbol{x}) = \frac{1}{h^2}\Phi\left(\frac{x}{h}\right)\Phi\left(\frac{y}{h}\right). \tag{11}$$

In the simulations, periodic boundary conditions were set along both x and y directions and the fast Fourier transform (FFT) method was employed to solve the matrix of the discretized governing equations.

The grid size of the discretized flow field was $dx = dy = 0.25$ μm, and the element for the dispersed immersed boundaries had half the size of fluid grid; i.e., $ds = 0.125$ μm. Time step was set to be 0.2 μs. Degree of liver sinusoid lumen stenosis (α) was defined as $1 - \mathrm{d_{sin}}/\mathrm{d_{cell}}$, where d_{sin} was the width of the narrowest part of the sinusoidal lumen and d_{cell} was the diameter of leukocyte (Fig. 1 *A*). Parameters used in the simulations are summarized in Table 1.

Simulation designs and analyses

Detailed features of the flow fields in both liver sinusoid lumen and Disse space were evaluated with or without the presence of the leukocyte. The effects of endothelium permeability, stiffness of Disse space and leukocyte, and the stenosis ratio of sinusoid on the flow field were investigated for deciphering the mechanical differences of liver sinusoidal microenvironment between physiological and pathological conditions. Flow features, including velocity and pressure fields, tension distribution and permeation velocity profile along the endothelium layer, and WSS distribution along the hepatocyte layer, were illustrated, and dynamical evolution of these characteristics following the leukocyte trafficking along the liver sinusoid lumen are presented. Here the WSS was computed based on the velocity profile of second and third layers of grids above the hepatocyte layer, by using the equation WSS = μ*(u3 − u2)/Δy, where u3 and u2 were velocity of third and second grid layers, respectively, Δy was the y axis distance between the two layers, and μ was the fluid viscosity. Penetration velocities along the endothelium were smoothed by using moving average filter.

RESULTS

Flow field in a leukocyte-free liver sinusoid

The reliability of the IBM was verified by simulating of a pre-stretching bubble with elastic membrane in water. The numerical results of the dynamics for equilibrium showed that the pressure jump over membrane and the membrane tension satisfy the Laplace relationship as predicted theoretically (Fig. S1 *A* and *B*). The deformations of a red blood cell in the Poiseuille flow of a straight tube were also simulated and compared with different grid size settings (Fig. S1 *C* and *D*) (26).

The elaborative features of the flow field in liver sinusoid are far from clear because of the limitation of experimental techniques, and IBM-based simulations made up the shortage by offering detailed flow characteristics. The simulations of a cell-free liver sinusoid with sinusoidal lumen diameter under physiological conditions showed that the flow in the lumen yielded a Poiseuille-like transverse

TABLE 1 Parameters used in simulations

Symbol	Parameter	Value	Unit	Sources
Es_{rbc}	shear modulus of red blood cell	6×10^{-6}	N m^{-1}	(26)
Eb_{rbc}	bending modulus of red blood cell	9.8×10^{-19}	N m	(26)
Es_{end}	shear modulus of endothelium	0.5, 2, 4 $\times 10^{-3}$	N m^{-1}	(27)
Eb_{end}	bending modulus of endothelium	0.5, 2,4 $\times 10^{-16}$	N m	this study
Es_{leu}	shear modulus of leukocyte	0.3, 1.2, 2.4 $\times 10^{-3}$	N m^{-1}	(17,28,29)
Eb_{leu}	bending modulus of leukocyte	0.23, 0.92, 1.84 $\times 10^{-16}$	N m	(17,28–30)
k_{Diss}	constant for springs connecting endothelium and hepatocyte layer	0.15, 0.5, 2$\times 10^{3}$	N m^{-3}	(31,32)
k_{rep}	coefficient of repulsive force	1000	N m^{-2}	(33)
d_{rep}	interaction distance	0.51	μm	(17)
κ	permeability	0,1,10 $\times 10^{-17}$	m^2	(34–36)
h_{end}	mean thickness of endothelium	100	nm	(35)
k_{fix}	coefficient of targeted point restriction	1.25×10^{-4}	N m^{-3}	this study
k_{A}	coefficient of area conservation constrains	1000	N m^{-1}	this study
ρ, μ	density and viscosity of plasma	1000, 1.2	kg·m^{-3}, cP	(18)
dt, t	time step and simulation time	0.2, 0.1–1	μs, s	this study
dx, ds	grid size	0.25, 0.125	μm	this study
L, H	channel size	18 × 100	μm	this study
R_{leu}	radius of leukocyte	4.25	μm	(37)
α	stenosis degree	0.2, 0.3,0.4		(37)
h_0	base width of Disse space	1	μm	this study
f_{dri}	external driving force on fluid	1×10^{5}	N m^{-3}	this study
R_{e}	Reynolds number	0.005		this study

Notes: $k_{\mathrm{s}} = E_{\mathrm{s}}/\mathrm{d}s^2$, $k_{\mathrm{b}} = E_{\mathrm{b}}/\mathrm{d}s^2$.

velocity profile, while the flow velocity in the Disse space was relatively low (Fig. 2 *A*). The magnitude of transverse velocity in the lumen presented periodic features with larger value near the stenosis, whereas the velocity in the Disse space showed the opposite trend. Transverse velocity profiles at two vertical cross sections of the liver sinusoid typically corresponding to the narrowest and the widest lumen diameters are shown (Fig. 2 *B*). The sinusoid-shaped lumen also induced periodically varied fluid exchange between lumen and Disse space so that fluids penetrated into the Disse space along the incident flow surface and permeated back into the lumen along the backflow surface (Fig. 2 *E*). The gradual decline of inward penetration velocity along the main flow resulted from the increased pressure inside the Disse space and the decreased pressure in the lumen along the flow (Fig. 2 *E* and *F*, dashed lines with arrow), which was consistent with previous simulations of a porous-membrane-separated double-layered channel (25). Integration of the positive penetration velocity along the endothelium showed that the penetration flow rate through the Disse space was about 2.5×10^{-15} m^3/s (0.15 nL/min) in a 100-μm-long liver sinusoid with normal permeability of 1×10^{-16} m^2. Meanwhile, the tangential strain along the endothelium layer, corresponding to the shear stress of luminal surface of the endothelium, also showed periodic features with the strongest and weakest strains around the locations of the narrowest and the widest lumens, respectively (Fig. 2 *C*). WSS on the hepatocyte layer presented periodic increases around the locations of widest lumen (Fig. 2 *D*).

In brief, the simulation results indicated that the fluid exchange between lumen and Disse space, and the stresses exerted on hepatocyte layer, are closely regulated by topological structure of liver sinusoid. Besides the fenestrate-induced permeability, which is enhanced by the lack of basement membrane and weak interaction between neighboring LSECs, interspersing both KCs on endothelium and HSCs in Disse space also result in local bulges of sinusoidal lumen. These characteristics thus endow liver sinusoidal endothelium with high deformability and roughness. The periodically varied sinusoidal diameter set in the current model mimicked the roughness of liver endothelium. These periodic compressions and relaxations of endothelium associated with the blood flow enhanced the mass exchange between sinusoid lumen and Disse space, and the fluctuation of the flow in Disse space regulated the local WSS on hepatocyte layer. Although the lumen diameter of the liver sinusoid in vivo is not exactly the same as in the simulations, the coupling of mass transfer and flow fluctuation associated with the compression-relaxation of LSECs along the flow reflected a fundamental mechanism in liver sinusoids.

Liver diseases often induce pathological changes of liver sinusoidal in both structures and mechanical properties, such as the decrease of endothelium permeability with the fenestrate decrease or disappearance of LSECs, the increase of Disse space stiffness due to collagen deposition, and the increase of sinusoidal lumen stenosis due to LSEC swelling etc. The effects of these changes on the flow field were investigated. First, the increase of lumen stenosis from $\alpha = 0.1$, 0.2 to 0.3, 0.4 did not affect the endothelium permeability much (Fig. S2 *A*) but decreased the WSS on the hepatocyte layer, apparently locating at the narrowest lumen (Fig. S2 *B*) because the increase of Disse space

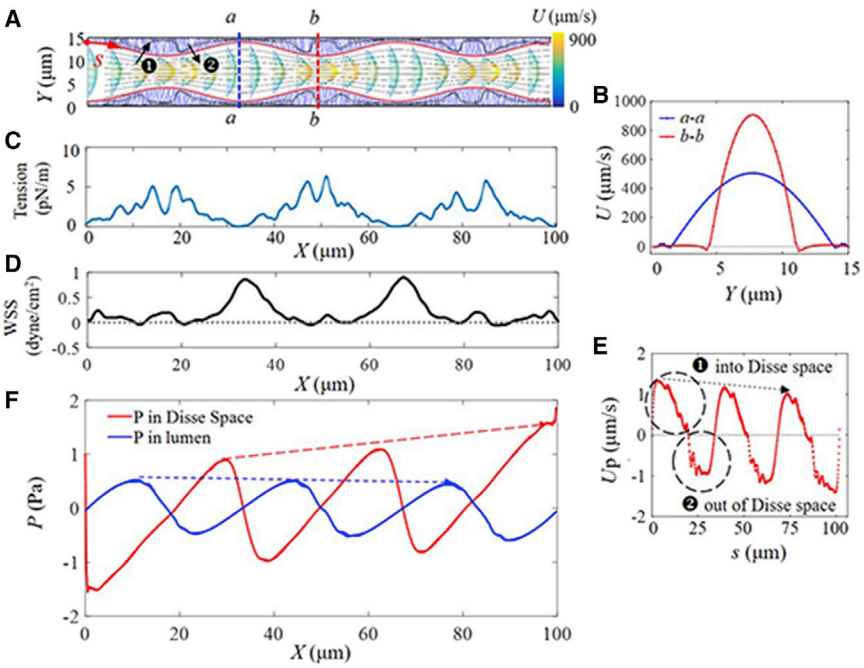

FIGURE 2 Flow-field features of liver sinusoid with permeable endothelium in absence of the leukocyte. (*A*) Streamlines of the velocity field and corresponding vector profiles. (*B*) Velocity profiles of two typical cross sections *a-a* and *b-b* as shown in (*A*). (*C*) Tension distribution along the upper endothelium as shown with the red arrow *S* in (*A*). (*D*) Wall shear stress (WSS) distribution along the upper hepatocyte layer. (*E*) Permeation velocity profile through the upper endothelium membrane from left to right end. Positive values represent flowing into the Disse space (❶) and negative values out to the sinusoidal lumen (❷). Dashed line with arrow shows the overall trend of declining inward penetration velocity results from increased pressure inside the Disse space and decreased pressure in the lumen along the flow direction. (*F*) Pressure distributions of both lumen and Disse space from left to right end with dashed lines showing the overall trends. Permeability of endothelium is set as 1×10^{-16} m^2, Disse space stiffness is 0.15 kPa, and stenosis degree of the sinusoidal lumen is $\alpha = 0.2$. To see this figure in color, go online.

thickness suppressed the radial velocity gradient (Fig. S2 *C*). Second, the increase of Disse space stiffness, represented using k_{Diss} of 0.15, 0.5, and 2.0 $\times$ 10^3 N/m^3 for normal (sD), fibrotic (mD), and cirrhotic (hD) cases (31,32), respectively, did not obviously change either the penetration velocity along the endothelium layer or WSS on the hepatocyte layer (Fig. S2 *D* and *E*). Third, the permeability of the endothelium layer significantly regulated the penetration velocity. The penetration velocity increased almost 10-fold proportionally around the central region with the increase of permeability from 1 $\times$ 10^{-17} m^2 to 1 $\times$ 10^{-16} m^2 (Fig. S2 *F*), but the scale of penetration velocity at the positions closing to both left and right ends of the sinusoid was less than the 10-fold increase. This deviation may be due to the effects of the closed boundary of the Disse space (25); i.e., the upright walls of the left and right sides of Disse space would hinder the nearby flow and decrease the penetration velocity. Correspondingly, mean WSS also increased slightly with the increase of endothelium permeability (Fig. S2 *G*). These results indicated that endothelium permeability is a key factor for regulating the flow field of liver sinusoid when leukocytes are absent.

Features of the flow field in a liver sinusoid with leukocytes

Narrow lumen diameter of about 7–15 μm and roughness in liver sinusoid inevitably results in the stressing of sinusoidal endothelium associated with the intra-lumen squeezing of blood cells, and this fluid-cell-boundary interaction affect the local flow field of liver sinusoid deterministically. To elucidate the effect of blood cell traveling on the flow fields of liver sinusoid, we first examined how the flow field in the Disse space and the penetration across the endothelium are altered when a leukocyte squeezes through the stenosis. The profiles of flow and penetration velocity showed that, when a leukocyte passed the maximum stenosis site, the fluid mostly penetrated into the Disse space through the contact zone and induced vortex in the Disse space nearby (Fig. 3 *A*). Further comparisons of pressure distribution and penetration velocity between the two moments while the leukocyte was just entering and leaving the stenosis showed that the enhancement of flow penetration into the Disse space had started from the moment when the leukocyte began to squeeze into the stenosis, which was consistent with relatively high pressure in the contact zone when the cell approached the stenosis (marked with red arrow) (Fig. 3 *B* and *C*, left). On the other hand, when the leukocyte was ejected from the narrow site, relatively low pressure appeared in the contact zone, which dragged the fluid out of the Disse space (marked with red arrow head) (Fig. 3 *B* and *C*, right). During the entire process of the leukocyte passing through the sinusoid (Fig. 3 D_a), the WSS on the hepatocyte layer was dynamically altered. Comparisons of WSS distributions for sequential five typical positions of the leukocyte trafficking through a sinusoid indicated a "massage" effect on the hepatocyte layer (Fig. 3 $D_{b\text{-}f}$). When the cell traveled in

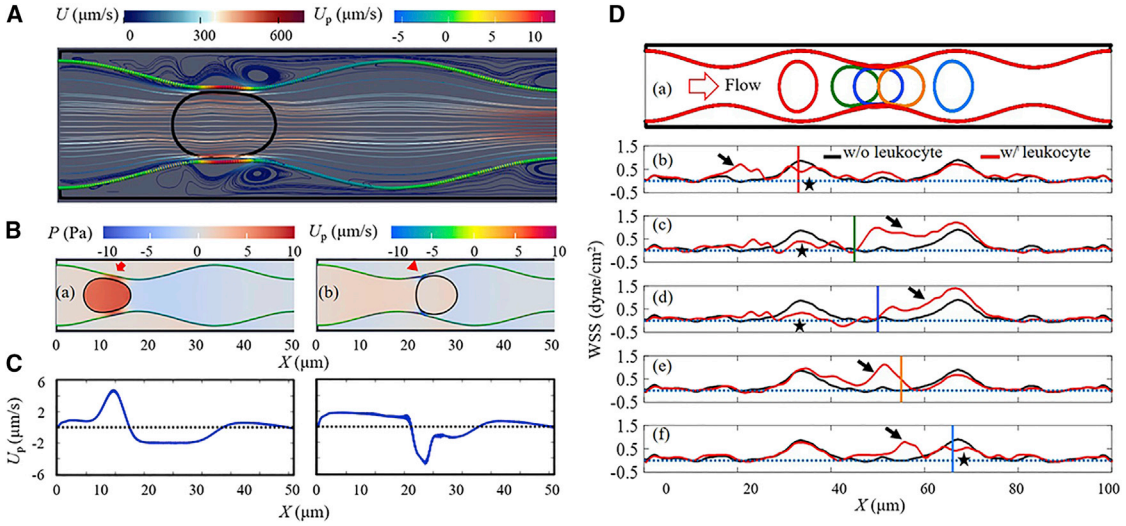

FIGURE 3 Effect of leukocyte trafficking on the flow penetration through endothelium. (*A*) Distributions of flow velocities in both sinusoidal lumen and Disse space and of permeation velocity through endothelium when the leukocyte is fully squeezed at the stenosis site. (*B*) Differences of pressure distribution and permeation velocity between two moments of leukocyte entering (*arrow*) and leaving (*arrowhead*) lumen stenosis. (*C*) Corresponding quantitative profiles of permeation velocity through endothelium at the two typical moments in (*B*). (*D*) Five representative positions of the leukocyte trafficking along sinusoidal lumen (*a*) and corresponding WSS distributions (red lines) on hepatocyte layer (*b–f*). WSS distribution in the absence of the leukocyte (black lines) serves as control and is also presented for comparison. Significant increased and decreased regions relative to the control are respectively marked with arrows and stars. Vertical line in each panel represents horizontal position of the leukocyte centroid. The parameters are set to be the permeability of endothelium of 1 $\times$ 10^{-16} m^2, stenosis degree of α = 0.2, Disse space stiffness of 0.15 kPa, and leukocyte stiffness of 1.2 $\times$ 10^{-3} N/m. To see this figure in color, go online.

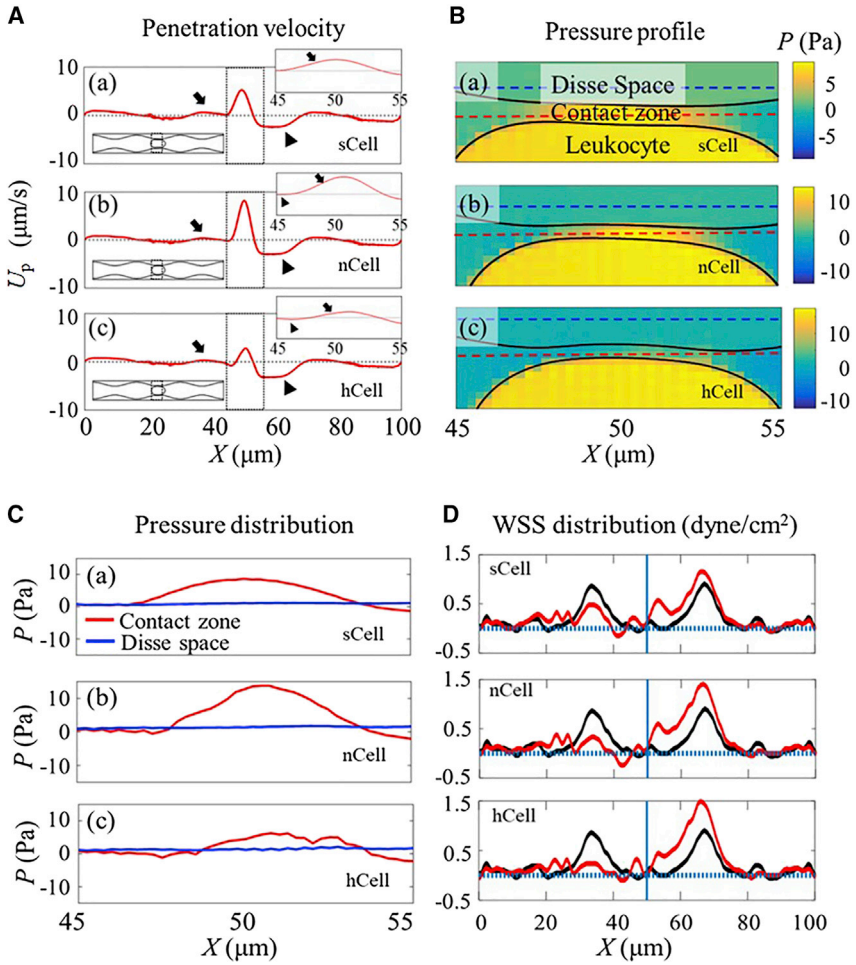

FIGURE 4 Effects of leukocyte stiffness on endothelium permeability and WSS on hepatocyte layer. (*A*) Penetration velocity along the upper endothelium when leukocyte is located at the middle of the liver sinusoid. From top to bottom are results for softened (sCell), normal (nCell), and hardened cell (hCell). Arrow and arrowhead depict the flow penetration into Disse space and out to sinusoidal lumen, respectively. Inserts at the top right corner of each panel are zoomed views of the selected rectangle zone in the middle. Relative positions of the leukocyte in the sinusoid are shown with the inserts at the bottom left corners. (*B*) Corresponding pressure profiles around the contact zones between leukocyte and endothelium for three types of leukocyte. Contact zone refers to the space where the distance between the leukocyte membrane and the endothelium layer was no larger than the interaction distance d_{rep} of 0.51 μm. The two black lines in each pressure profile represent the endothelium layer (*upper*) and the top edge of leukocyte (*lower*), respectively, which are the same in other figures if not indicated otherwise. (*C*) Quantitative pressure distributions along the contact zone (*red dashed line in B*) and in the Disse space(*blue dashed line in B*). (*D*) Corresponding WSS distributions (*red lines*) along the hepatocyte layer, with the control distribution (*black line*) in the absence of the leukocyte. Vertical blue line represents the horizontal position of the leukocyte centroid. The parameters are set to be the permeability of endothelium of 1×10^{-16} m^2, stenosis degree of $\alpha = 0.2$, and Disse space stiffness of 0.15 kPa. To see this figure in color, go online.

lumen with wider diameter, upstream WSS was increased and nearby WSS was decreased (Fig. 3 D_b). The downstream WSS on the hepatocyte layer was significantly upregulated and that of upstream presented a contradictory trend while leukocyte was squeezing into the stenosis (Fig. 3 $D_{c\text{-}d}$). The upstream WSS was significantly enhanced when the leukocyte was forced to leave the stenosis (Fig. 3 D_e), until the next cycle (Fig. 3 D_f). Mean penetration flow rate through the endothelium was about 0.16 nL/min, just a little higher than a cell-free sinusoid in the entire process of leukocyte trafficking but more effective interchange between nutrient materials from blood flow and metabolic substance secreted by hepatocytes. Meanwhile, leukocyte trafficking along the liver sinusoid induced distinct WSS modes on the hepatocyte layer. WSS distribution along the hepatocyte layer was quasi-static in the absence of the leukocyte with different magnitudes at distinct positions. In contrast, a leukocyte traveling in the sinusoid induced dynamic WSS distributions at each site, indicating that WSS suffered by physiological hepatocyte layer fluctuates periodically upon both location and time.

Effects of leukocyte and Disse space stiffnesses on flow field

Leukocytes present various mechanical properties with altered stiffness under different stimuli (14,15). To explore how the mechanical properties of leukocytes influence the penetration through permeable endothelium and the shear stress on hepatocyte layer, we chose three different stiffnesses of 0.3×10^{-3}, 1.2×10^{-3}, and 2.4×10^{-3} N/m for representing the softened (sCell), normal (nCell), and hardened cell (hCell), respectively (17,28,29). Results showed that the leukocyte stiffness regulated the penetration velocity profile, especially at the location of stenosis (Fig. 4 *A*). Soft leukocyte at the stenosis induced the fluid in the entire contact zone to penetrate through the porous endothelium into the Disse space and penetrate out into the lumen in the downstream, where the upstream almost kept zero penetration (Fig. 4 A_a). With the increase of leukocyte stiffness to nCell (Fig. 4 A_b) or hCell (Fig. 4 A_c), the trends of penetration velocity profile were similar to those of sCell, but the penetration magnitude in the contact zone was higher for nCell than for hCell or sCell. In addition,

the upstream contact region presented slight fluid penetration out of the Disse space for both nCell and hCell (Fig. 4 A_b and A_c, arrowheads of inserts). In fact, it was the pressure distributions around the contact region that determined the penetration velocity profiles. Both pressure profiles around the contact zone (Fig. 4 *B*) and pressure distributions along typical lines (Fig. 4 *C*) demonstrated that the squeezed stiff leukocyte induced two inversions around both upstream and downstream of the contact zone but only one inversion around the downstream of the contact zone for the soft leukocyte; that is, the pressures of sinusoidal lumen around the two ends of contact zone were smaller than those of Disse space and the pressure in the central contact zone presented the opposite trend. Corresponding WSSs on the hepatocyte layer induced by leukocyte squeezing in the stenosis were also different in magnitude; that is, the stiffer nCell or hCell induced a higher WSS fluctuation with higher downstream WSS and weaker upstream WSS than for sCell (Fig. 4 *D*). Dynamic evolutions of WSS following the leukocyte traveling to different position along the sinusoid demonstrated that the stiffer cell induced stronger massage effect on the hepatocyte layer with larger variations of WSS magnitude (Fig. S3 *A–D*), which was consistent with higher fluctuations of WSS with time and higher peak WSS for nCell and hCell (Fig. S3 *E* and *F*).

The effect of Disse space stiffness was also investigated upon the same settings of k_{Diss} as 0.15, 0.5, and 2.0×10^3 N/m^3. Results showed that the pressure difference between lumen and Disse space around the contact zone was the highest for the normal case of sD (Fig. 5 *B*, left column). The pressure profile along the contact zone also showed different trends upon the change of Disse space stiffness. For the normal case of sD, the lumen pressure increased gradually from the baseline around the upstream to maximum at the center of the contact zone and then decreased below the baseline around the downstream. However, those of mD and hD exhibited multiple increase-decrease transitions, and the stiffer the Disse space the more transitions around the central contact zone (Fig. 5 *B*). Again, the difference of pressure profile induced different penetration velocity profile along the endothelium. The fluid penetrated into the Disse space with positive U_p along the contact zone and back out into the lumen with negative U_p in the downstream for the case of sD. The stiffer Disse space induced two phases with penetrating out first from Disse space into lumen along the left half part of the contact region and then reverse penetration direction along the right half region. Corresponding penetration velocity magnitude was smaller for both mD and hD than that of sD (Fig. 5 *A*). The weak penetration for hD led to almost the same WSS on the hepatocyte layer as that of cell-free sinusoid. In other words, the stiffer Disse space decreased the massage effect when a leukocyte was traveling through a liver sinusoid (Fig. 5 *C*).

The above results showed that the effects of leukocyte and Disse space stiffness on the flow features were opposite; i.e., increasing leukocyte stiffness enhanced the massage effect on the hepatocyte layer. but increasing Disse space stiffness weakened the massage effect by downregulating the corresponding penetration velocity profile along the endothelium and WSS along the hepatocyte layer. Thus, combination of these two factors showed that penetration velocity distribution in the contact zone was regulated by the stiffness of both the leukocyte and the Disse space (Fig. 6), which was again determined by those pressure distribution profiles (Fig. S4). For soft leukocyte, the penetration through endothelium in the contact zone was unidirectional and the velocity value was almost the same regardless of the stiffness of Disse space (Fig. 6 *B*) on the comparable pressure profiles (Fig. S4 *A*). This feature was also kept for the combination of nCell and sD (Figs. 6 *C*, red; S4 *B*, left column). By contrast, all the other cases generated bidirectional

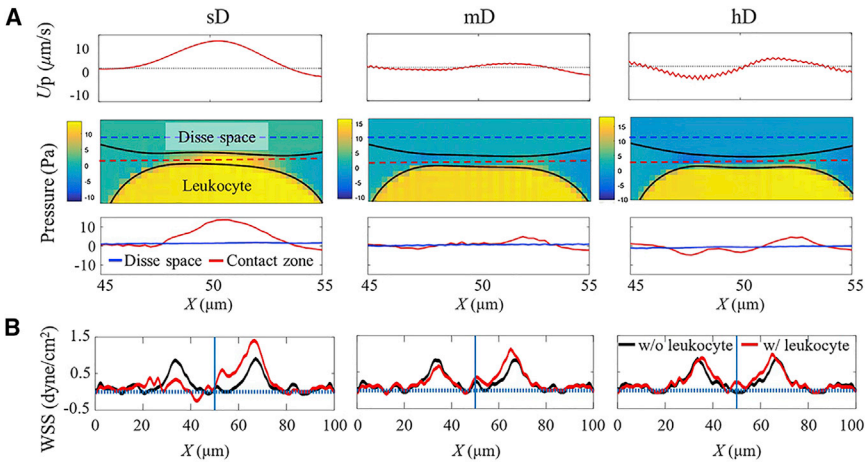

FIGURE 5 Effects of Disse space stiffness on endothelium permeability and WSS on hepatocyte layer. (*A*) Penetration velocity along the upper endothelium of the contact zones. From left to right are results for normal (sD), medium (mD), and high (hD) matrix stiffness in Disse space that mimic normal, fibrotic, and cirrhotic liver, respectively. (*B*) Corresponding pressure profiles (*upper row*) around the contact zones between leukocyte and endothelium and quantitative pressure distributions (*lower row*) along the contact zone (*red dashed line in upper row*) and in the Disse space (*blue dashed line in upper row*). (*C*) Corresponding WSS distributions (*red lines*) along the hepatocyte layer, with the control distribution (*black line*) in the absence of the leukocyte. Vertical blue line represents the horizontal position of the leukocyte centroid. The parameters are set to be the permeability of endothelium of 1×10^{-16} m^2, leukocyte stiffness of 1.2×10^{-3} N/m, and stenosis degree of $\alpha = 0.2$. To see this figure in color, go online.

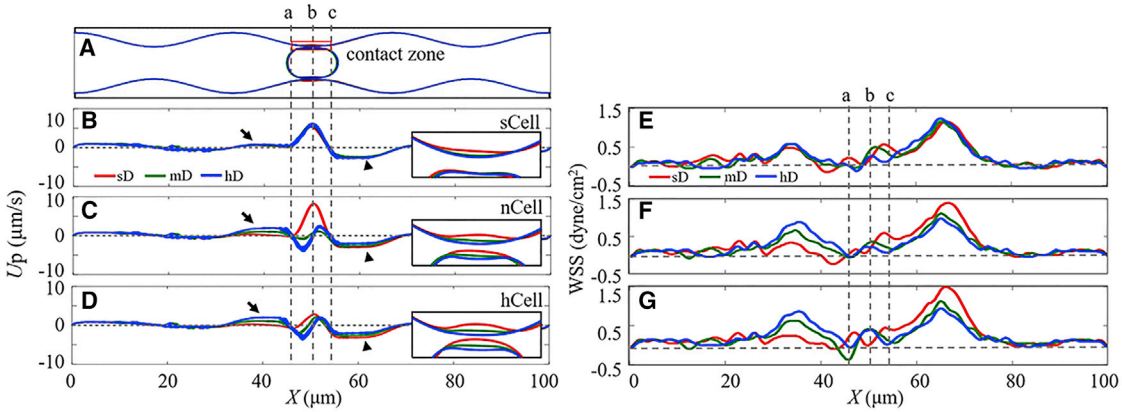

FIGURE 6 Cooperative roles of leukocyte and Disse space stiffnesses in regulating endothelium penetration and WSS on hepatocyte layer. (*A*) Configuration of a normal stiffness leukocyte (nCell) at the center of stenosis under different stiffnesses of Disse space. (*B–D*) Penetration velocity distributions along the upper endothelium membrane induced by a squeezed leukocyte with different cellular stiffnesses of sCell (*B*), nCell (*C*), or hCell (*D*). Red, green, and blue lines denote the results for Disse space stiffnesses of sD, mD, and hD, respectively. Inserts in (*B*)–(*D*) are zoomed views of contact zones as marked with red rectangle in (*A*). Arrows and arrowheads depict the flow penetration into Disse space and out to sinusoidal lumen, respectively. (*E–G*) WSS distributions along the upper hepatocyte wall induced by squeezed leukocytes with different cellular stiffnesses of sCell (*E*), nCell (*F*), or hCell (*G*). The parameters are set to be the permeability of endothelium of 1×10^{-16} m^2 and stenosis degree of $\alpha = 0.2$. To see this figure in color, go online.

penetrations along the contact zone with slight change of penetration velocity magnitude (Fig. 6 *C*, green and blue lines; *D*), resulting from the inversion of pressure difference between lumen and Disse space around the contact zone (Fig. S4 *B*, right two columns; *C*). Those penetration profiles of the two ends beyond the contact zone also displayed different modes upon different combinations.

In brief, both the penetration mode and the magnitude were regulated comprehensively by the mechanical properties of both leukocyte and sinusoid. Interestingly, the combination of both normal leukocyte (nCell) and Disse space (sD) induced the largest penetration velocity along the contact zone with direction of penetrating into the Disse space (Fig. 6 *C*, red line), indicating the physiological significance of mechanical properties of both leukocyte and liver sinusoid, as well as their matching. This observation was further supported by WSS distributions from the two stiffnesses combination. Although profiles of WSS on hepatocytes were similar for sCell cases, the WSS profiles around the contact zone appeared to show an obvious trend for the combinations of nCell or hCell with different stiffnesses of Disse space; that is, the higher the Disse space stiffness, the higher and lower the WSS at upstream and downstream, respectively, which is close to that of the cell-free case (Fig. 6 *E–G*). Results indicated that the matching of leukocyte and Disse space stiffnesses could enhance the massage effect of blood flow on hepatocyte layer. The stiffer Disse space, presented under fibrotic or cirrhotic conditions, would shield the sensation of pressure imposed by leukocyte squeezing at the stenosis and lose most of the ability to regulate the local WSS on the hepatocyte layer, further implying that this dynamical regulation of WSS may be important to the hepatocyte function.

Effects of endothelium permeability and stenosis of sinusoid lumen on flow field

Defenestration was found both in elderly rat liver and in liver endothelial cells cultured in vitro (38), as well as in the progress of liver fibrosis and cirrhosis (39), which is bound to decrease the endothelium permeability. To explore the effect of endothelium permeability on sinusoidal flow field, we set the permeability to 1.0×10^{-17} and 1.0×10^{-16} m^2 for representing the defenestration and normal conditions, respectively (34–36). Results showed that the permeability of the endothelium layer significantly regulated the fluid penetration velocity. The penetration velocity reached maximum value when the leukocyte was squeezed at every stenosis (Fig. 7 *A*), which was less than 10-fold the permeability of 1.0×10^{-16} m^2 relative to that of 1.0×10^{-17} m^2 (Fig. 7 *A*, the third and fourth rows). Although the endothelium permeability significantly regulated the penetration velocity, corresponding WSSs on the hepatocyte layer were slightly enhanced just 1.19- to 1.42-fold (Fig. 7 *B*).

Inflammation occasionally causes LSEC swelling and increases the stenosis extent of the liver sinusoid lumen. We explored the effects of liver endothelium swelling on the flow field of liver sinusoid by increasing the stenosis extent from 0.2 to 0.3. Results showed that the increase of stenosis degree did not affect the penetration velocity much when a leukocyte was traveling along the sinusoid (Fig. 8 *A*) except when the leukocyte was just squeezed in the stenosis, where the increase of lumen stenosis extent significantly decreased the penetration velocity around the leukocyte location (Fig. 8 *A*, the third left row). By contrast, small WSS variations upon the stenosis change indicated that the stenosis extent did not affect WSS much (Fig. 8 *B*).

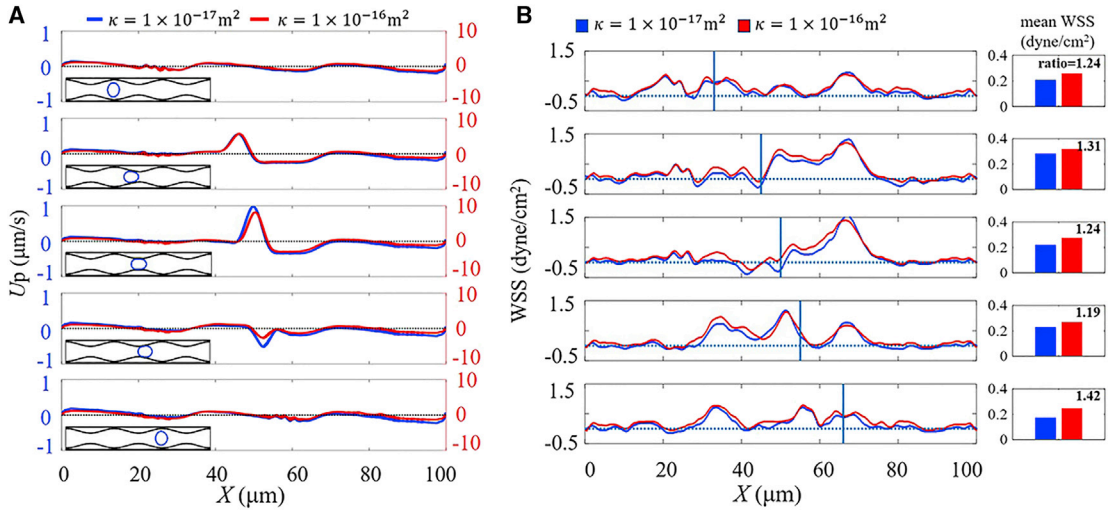

FIGURE 7 Effect of endothelium permeability on endothelium penetration and WSS on hepatocyte layer. (*A*) Typical penetration velocity distributions of sinusoid at different leukocyte positions (inserts) for both normal permeability of $\kappa = 1 \times 10^{-16}$ m^2(*red lines*) and defenestrated permeability of $\kappa = 1 \times 10^{-17}$ m^2(*blue lines*). (*B*) Corresponding WSS distributions on hepatocyte layer. Vertical blues lines represent the positions of cell centroid. Inserts show mean WSS along hepatocyte layer with indicated ratio of high-permeability WSS to low-permeability WSS. Other parameters are set to be stenosis degree of $\alpha = 0.2$, Disse space stiffness of 0.15 kPa, and leukocyte stiffness of 1.2×10^{-3} N/m. To see this figure in color, go online.

Both decrease of endothelial permeability induced by defenestration of LSECs (7) and stiffening of Disse space induced by HSC secreted matrix deposition (8) usually accompany each other in the progress of liver fibrosis and cirrhosis, and the activation of HSCs also enhances the stenosis of liver lumen. Based on the above considerations, we further explored the combined effects of ECM stiffness, stenosis extent, and endothelium permeability, which is typically the case in liver cirrhosis (40). Results showed that, in a cirrhotic sinusoid, penetration velocity decreased significantly while a leukocyte was traveling through the sinusoid, and WSS on the hepatocyte layer decreased by about 40% during the whole process (Fig. 8 *C* and *D*).

DISCUSSION

Elaborative flow features in liver sinusoid were far from clear because of the limitation of experimental techniques. Although the effects of endothelium permeability, roughness of hepatocyte microvilli, and collagen layer of Disse space on the sinusoidal flow were numerically investigated by treating them as a porous and permeable medium in an in vitro hepatic sinusoidal model, the regulation roles of endothelium roughness, the stiffness of Disse space induced by collagen deposition, as well as the presence of leukocyte squeezing on sinusoidal flow are still unclear (41). Here we investigated numerically the flow field, including velocity and pressure distributions of all regions, penetration velocity along the endothelium, and WSS along the hepatocyte layer in a leukocyte-free or a leukocyte-presenting liver sinusoid. The effects of both leukocyte and Disse space stiffnesses, endothelium permeability, and lumen stenosis on the flow were also explored. Results showed that all the factors manipulate flow penetration through endothelium and WSS on hepatocytes with different sensitivities and trends (Table S1). The distribution of WSS along the hepatocyte layer was not uniform in a leukocyte-free liver sinusoid because of the periodically varied sinusoidal lumen diameter. The intermittent squeezing into and ejecting out of the stenosis of leukocyte further enhanced the exchange of flow between lumen and Disse space and induced dynamic changes of WSS along hepatocyte layer like a massage effect. Proper adjustment of higher leukocyte stiffness and softer Disse space stiffness enhanced this massage effect. Separated change of endothelium permeability significantly regulated penetration velocity along endothelium layer, whereas the WSS magnitude along the hepatocyte layer and dynamic massage effect changed mildly. These results offered new insights into uncovering the elaborate flow features in a liver sinusoid and its corresponding change under pathological progress.

Multiple mechanical and physical factors regulate the luminal flow and the interstitial flow features in a leukocyte-free liver sinusoid, including the endothelium elasticity and permeability, the sinusoidal topography, and the elasticity and permeability of Disse space. Flow in the sinusoidal lumen presents a Poiseuille-like velocity profile, and periodically changes its magnitude along the flow direction due to the periodic variations of lumen diameter. Blood serum penetrates into the Disse space as the lumen is narrowing and out of the Disse space as the lumen is expanding, which suggests that varying the diameter is a mechanism for liver to enhance its ability of substance exchange between the lumen and the Disse space. Although the topographical setting of sinusoidal endothelium in this work was ideal to be comparable with in vivo features, it is still meaningful

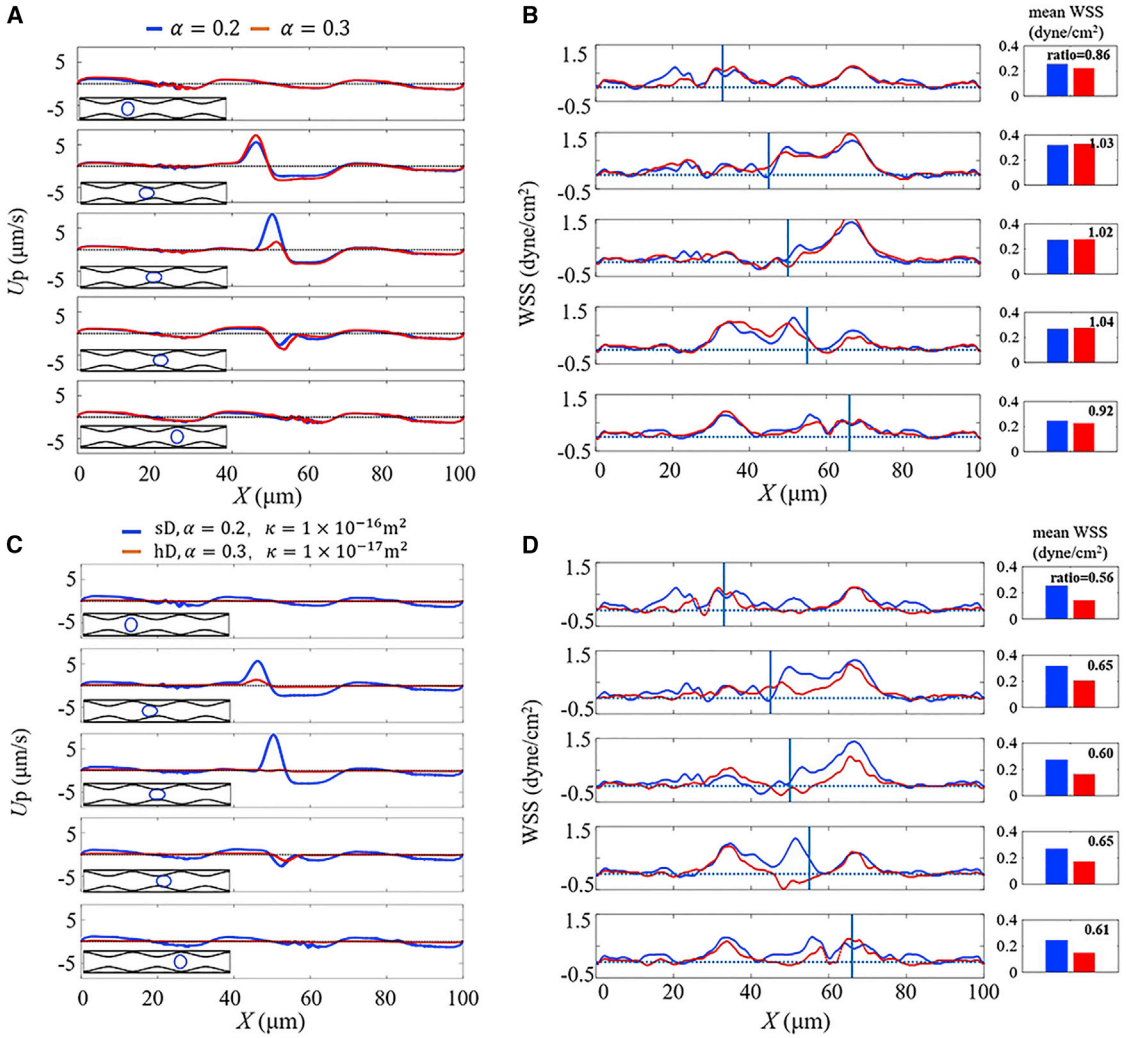

FIGURE 8 Cooperative effects of lumen stenosis, Disse space stiffness, and endothelium permeability on endothelium penetration and WSS on hepatocyte layer. (*A* and *C*) Typical penetration velocity distributions of sinusoid at different leukocyte positions (inserts) for both stenoses of $\alpha = 0.2$ (*blue lines*) and $\alpha = 0.3$ (*red lines*) (*A*) or for a normal (*blue lines*) with endothelium permeability of 1×10^{-16} m^2 and a cirrhotic sinusoid (*red lines*) with endothelium permeability of 1×10^{-17} m^2 (*C*). (*B* and *D*) WSS distributions on hepatocyte layer corresponding to (*A*) and (*C*), respectively, with vertical blue lines representing the positions of cell centroid and inserts showing mean WSS along the hepatocyte layer with indicated ratio of high- to low-stenosis WSS. Other parameters are set to Disse space stiffness of 0.15 kPa, leukocyte stiffness of 1.2×10^{-3} N/m, and permeability of 1×10^{-16} m^2 in (*A*) and (*B*) and leukocyte stiffness of 1.2×10^{-3} N/m in (*C*) and (*D*). To see this figure in color, go online.

to estimate the fundamental flow features. On the one hand, all the LSECs, KCs, and HSCs have the ability to locally alter the diameter of liver sinusoid (42). On the other hand, experimental measurements of leukocyte flow in individual sinusoids of rat liver shows that the velocity varies a wide range (37). Thus, these observations propose to a certain extent the heterogeneity in the diameter of an individual liver sinusoid.

It is known that cells traveling in microcirculation exert forces on the vessel wall through plasma (43). We speculated that the appearance of leukocytes should temporarily alter the microenvironment in the sinusoid, especially when it is squeezing through the lumen with stenosis, influence plasma penetration through the porous sinusoidal endothelium, and eventually affect the flow dynamics in the Disse space. In general, when leukocytes pass through the liver sinusoid, WSSs on hepatocytes are dynamically regulated. Leukocyte squeezing through liver sinusoid enhances the interstitial flow in Disse space and the shear stress exposed to the hepatocytes, presenting a massage effect. Independent change of leukocyte stiffness alone or combined changes with other factors would regulate the flow characteristics of liver sinusoid, as exemplified by only combination of normal leukocyte (nCell) and Disse space (sD) stiffnesses exhibiting optimal penetration velocity and massage effect (Fig. 6).

Physiological functions of hepatocytes are known to be regulated by shear stress in in vitro experiments (44–46). To our knowledge, however, the actual shear stress generated by blood flow acting on the hepatocyte layer is still

unknown, since the hepatocytes are kept out of direct contact with the blood stream. Although these cells are separated from the main stream of blood flow by the thin sinusoidal endothelium, the penetration-generated flow in the Disse space may apply shear stress to the hepatocyte surface. This is mainly attributed to the specialized fenestrae of LSECs that allow blood flow to partially penetrate into and out of the Disse space. Our previous numerical work applied a porous-membrane-separated double-layered channel to partially mimic the fenestrated structures of the liver sinusoid, indicating that the shear stress acting on the lower channel surface (corresponding to the hepatocytes here) is regulated by the permeability of the porous membrane and the size of channel (25). We further tested here the effects of the permeability of the endothelium on the shear stress on the hepatocyte surface based on a model mimicking in vivo structural size and mechanical environment. Noting that the interstitial flow in the Disse space is still unable to be measured experimentally, these numerical outputs from this work provided a basic understanding for what it looks like and to what extent it could be regulated by various mechanical and physical factors.

It should be noted that the current modeling of liver sinusoid and corresponding simulations was simplified in this study. On the one hand, the endothelium layer was assumed to be a thin layer with thickness of 0.1 μm only for permeability assessment based on Darcy's law, and the interplay between permeable flow and endothelium layer was neglected here. In fact, this interplay between permeable flow and endothelium layer could not be ignored if it is simulated with realistic thickness of 2–3 μm, as shown in the literature (47–49). On the other hand, this study did not set slip velocity on the endothelium layer, even though most blood vessels, especially smaller veins or blood capillaries, present the behavior of slip velocity on the vessel wall (50), and this existence of slip velocity will affect flow field (50–52). This simplification was mainly based on the consideration that the presence of slip velocity on the endothelium or not or the extent of slip velocity is still not clear experimentally for the liver sinusoid, and inappropriate setting of slip velocity on the endothelium in the simulations may result in larger errors than those on no-slip velocity setups. Evidently, future optimizations are needed for more accurate presentation of flow field in the liver sinusoid. In addition, this study only focused on the effect of leukocyte trafficking on flow field of liver sinusoid. More complicated simulations, including adhesion dynamics of leukocytes as well as substance diffusion that happen in in vivo environments, need further extension of the IBM (53).

CONCLUSIONS

By performing numerical modeling based on IBM, this study showed that higher endothelial permeability, smaller Disse space elasticity, and normal leukocyte elasticity cooperatively enhance fluid penetration across endothelium and WSS on hepatocyte layer. In addition, flow-forced leukocyte squeezing along sinusoid lumen due to the roughness of endothelium surface can massage the hepatocyte layer through dynamic endothelium permeability but does not alter flow significantly. This study made up the limitations of current experimental techniques and offered the detailed profiles of sinusoidal flow field, which are evidently critical in elucidating the mass transportation mechanism of Disse space and the effect of flow on hepatocyte functions. Furthermore, this study also offers references for developing an in vitro liver microfluidic chip that mimics in vivo sinusoidal flow features.

SUPPORTING MATERIAL

Supporting material can be found online at https://doi.org/10.1016/j.bpj.2022.10.022.

AUTHOR CONTRIBUTIONS

S.C., S.L., and M.L. designed the research and wrote the article. S.C., J.Z., and X.G. performed the IBM simulations and analyzed the data. X.W., P.J., L.Z., Y.C., T.W., and X.G. analyzed the data. J.X. conducted the dimensionless analysis.

ACKNOWLEDGMENTS

All simulations were performed on the National Supercomputer Center in Tianjin. This work was supported by National Natural Science Foundation of China grants (32130061, 11972042,and 12072198), and Scientific Instrument Developing Project of Chinese Academy of Sciences grant GJJSTU20190005.

DECLARATION OF INTERESTS

The authors declare no competing interests.

REFERENCES

1. Aird, W. C. 2007. Phenotypic heterogeneity of the endothelium: II. Representative vascular beds. *Circ. Res.* 100:174–190.
2. Vollmar, B., and M. D. Menger. 2009. The hepatic microcirculation: mechanistic contributions and therapeutic targets in liver injury and repair. *Physiol. Rev.* 89:1269–1339.
3. Richardson, P. D., and P. G. Withrington. 1981. Liver blood flow. Effect of drugs and hormones on liver blood flow. *Gastroenterology.* 81:356–375.
4. Richardson, P. D., and P. G. Withrington. 1981. Liver blood flow. I. Intrinsic and nervous control of liver blood flow. *Gastroenterology.* 81:159–173.
5. Song, Z., K. Gupta, …, H. Yu. 2017. Mechanosensing in liver regeneration. *Semin. Cell Dev. Biol.* 71:153–167.
6. Pradhan, S., O. A. Banda, …, J. H. Slater. 2020. Biofabrication strategies and engineered in vitro systems for vascular mechanobiology. *Adv. Healthc. Mater.* 9:e1901255.

7. Szafranska, K., L. D. Kruse, …, B. Zapotoczny. 2021. The wHole story about fenestrations in LSEC. *Front. Physiol.* 12:735573.
8. Wells, R. G., P. C. Georges, …, R. G. Wells. 2005. The role of matrix Stiffness in hepatic stellate cell activation and liver fibrosis. *J. Clin. Gastroenterol.* 39:S158–S161.
9. Sheth, K., and P. Bankey. 2001. The liver as an immune organ. *Curr. Opin. Crit. Care.* 7:99–104.
10. Jenne, C. N., and P. Kubes. 2013. Immune surveillance by the liver. *Nat. Immunol.* 14:996–1006.
11. Kita, H., I. R. Mackay, …, M. E. Gershwin. 2001. The lymphoid liver: considerations on pathways to autoimmune injury. *Gastroenterology.* 120:1485–1501.
12. Maas, S. L., O. Soehnlein, and J. R. Viola. 2018. Organ-specific mechanisms of transendothelial neutrophil migration in the lung, liver, kidney, and aorta. *Front. Immunol.* 9:2739.
13. Mccuskey, R. S. 2000. Morphological mechanisms for regulating blood flow through hepatic sinusoids. *Liver.* 20:3–7.
14. Worthen, G. S., B. Schwab, …, G. P. Downey. 1989. Mechanics of stimulated neutrophils: cell stiffening induces retention in capillaries. *Science.* 245:183–186.
15. Fay, M. E., D. R. Myers, …, W. A. Lam. 2016. Cellular softening mediates leukocyte demargination and trafficking, thereby increasing clinical blood counts. *Proc. Natl. Acad. Sci. USA.* 113:1987–1992.
16. Peskin, C. S. 2003. The immersed boundary method. *Acta Numer.* 11:479–517.
17. Wu, T., and J. J. Feng. 2015. Modeling the mechanosensitivity of neutrophils passing through a narrow channel. *Biophys. J.* 109:2235–2245.
18. Lenarda, P., A. Coclite, and P. Decuzzi. 2019. Unraveling the vascular fate of deformable circulating tumor cells via a hierarchical computational model. *Cell. Mol. Bioeng.* 12:543–558.
19. Ju, M., S. S. Ye, …, S. Kim. 2015. A review of numerical methods for red blood cell flow simulation. *Comput. Methods Biomech. Biomed. Eng.* 18:130–140.
20. Rejniak, K. A. 2012. Investigating dynamical deformations of tumor cells in circulation: predictions from a theoretical model. *Front. Oncol.* 2:111.
21. Strychalski, W., C. A. Copos, …, R. D. Guy. 2015. A poroelastic immersed boundary method with applications to cell biology. *J. Comput. Phys.* 282:77–97.
22. Battista, N. A., W. C. Strickland, …, L. A. Miller. 2018. IB2d Reloaded: a more powerful Python and MATLAB implementation of the immersed boundary method. *Math. Methods Appl. Sci.* 41:8455–8480.
23. Battista, N. A., W. C. Strickland, and L. A. Miller. 2017. IB2d: a Python and MATLAB implementation of the immersed boundary method. *Bioinspiration Biomimetics.* 12:036003.
24. Kim, Y., and C. S. Peskin. 2006. 2-D parachute simulation by the immersed boundary method. *SIAM J. Sci. Comput.* 28:2294–2312.
25. Chen, S., J. Xue, …, M. Long. 2020. Flow field analyses of a porous membrane-separated, double-layered microfluidic chip for cell co-culture. *Acta Mech. Sin.* 36:754–767.
26. Tomaiuolo, G. 2014. Biomechanical properties of red blood cells in health and disease towards microfluidics. *Biomicrofluidics.* 8:051501.
27. Suki, B., Y. Hu, …, E. Bartolák-Suki. 2017. A microfluidic chamber-based approach to map the shear moduli of vascular cells and other soft materials. *Sci. Rep.* 7:2305.
28. Barber, J., and L. Zhu. 2019. Two-dimensional finite element model of breast cancer cell motion through a microfluidic channel. *Bull. Math. Biol.* 81:1238–1259.
29. Jadhav, S., C. D. Eggleton, and K. Konstantopoulos. 2005. A 3-D computational model predicts that cell deformation affects selectin-mediated leukocyte rolling. *Biophys. J.* 88:96–104.
30. Zhelev, D. V., D. Needham, and R. M. Hochmuth. 1994. A novel micropipet method for measuring the bending modulus of vesicle membranes. *Biophys. J.* 67:720–727.
31. Du, Y., N. Li, and M. Long. 2018. Liver sinusoid on a chip. *Methods Cell Biol.* 146:105–134.
32. Desai, S. S., J. C. Tung, …, T. T. Chang. 2016. Physiological ranges of matrix rigidity modulate primary mouse hepatocyte function in part through hepatocyte nuclear factor 4 alpha. *Hepatology.* 64:261–275.
33. Dong, C., and R. Skalak. 1992. Leukocyte deformability: finite element modeling of large viscoelastic deformation. *J. Theor. Biol.* 158: 173–193.
34. Braet, F., and E. Wisse. 2002. Structural and functional aspects of liver sinusoidal endothelial cell fenestrae: a review. *Comp. Hepatol.* 1:1.
35. Svistounov, D., A. Warren, …, V. C. Cogger. 2012. The relationship between fenestrations, sieve plates and rafts in liver sinusoidal endothelial cells. *PLoS One.* 7:e46134.
36. Warren, A., V. C. Cogger, …, D. G. Le Couteur. 2010. Liver sinusoidal endothelial fenestrations in caveolin-1 knockout mice. *Microcirculation (Phila.).* 17:32–38.
37. Komatsu, H., A. Koo, and P. H. Guth. 1990. Leukocyte flow dynamics in the rat liver microcirculation. *Microvasc. Res.* 40:1–13.
38. Fraser, R., V. C. Cogger, …, D. G. Le Couteur. 2012. The liver sieve and atherosclerosis. *Pathology.* 44:181–186.
39. Zhou, W. C., Q. B. Zhang, and L. Qiao. 2014. Pathogenesis of liver cirrhosis. *World J. Gastroenterol.* 20:7312–7324.
40. Friedman, S. L. 2003. Liver fibrosis – from bench to bedside. *J. Hepatol.* 38:38–53.
41. Wang, T., S. Q. Lü, …, Y. Cui. 2021. Influence of microflow on hepatic sinusoid blood flow and red blood cell deformation. *Biophys. J.* 120:4859–4873.
42. McCuskey, R. S. 2008. The hepatic microvascular system in health and its response to toxicants. *Anat. Rec.* 291:661–671.
43. Freund, J. B., and J. Vermot. 2014. The wall-stress footprint of blood cells flowing in microvessels. *Biophys. J.* 106:752–762.
44. Xia, L., T. Arooz, …, H. Yu. 2012. Hepatocyte function within a stacked double sandwich culture plate cylindrical bioreactor for bioartificial liver system. *Biomaterials.* 33:7925–7932.
45. Kan, P., H. Miyoshi, and N. Ohshima. 2004. Perfusion of medium with supplemented growth factors changes metabolic activities and cell morphology of hepatocyte-nonparenchymal cell coculture. *Tissue Eng.* 10:1297–1307.
46. Dash, A., M. B. Simmers, …, B. R. Wamhoff. 2013. Hemodynamic flow improves rat hepatocyte morphology, function, and metabolic activity in vitro. *Am. J. Physiol. Cell Physiol.* 304:C1053–C1063.
47. Mori, Y., H. Chen, …, M. C. Calderer. 2013. A dynamic model of polyelectrolyte gels. *SIAM J. Appl. Math.* 73:104–133.
48. Verri, M., G. Guidoboni, …, R. Sacco. 2018. The role of structural viscoelasticity in deformable porous media with incompressible constituents: applications in biomechanics. *Math. Biosci. Eng.* 15:933–959.
49. Young, Y. N., Y. Mori, and M. J. Miksis. 2019. Slightly deformable Darcy drop in linear flows. *Phys. Rev. Fluids.* 4:063601.
50. Misra, J. C., and B. K. Kar. 1989. Momentum integral method for studying flow characteristics of blood through a stenosed vessel. *Biorheology.* 26:23–35.
51. Pal, D., N. Rudraiah, and R. Devanathan. 1988. The effects of slip velocity at a membrane-surface on blood-flow in the microcirculation. *J. Math. Biol.* 26:705–712.
52. Elshahed, M. 2004. Blood flow in capillary under starling hypothesis. *Appl. Math. Comput.* 149:431–439.
53. Dillon, R., L. Fauci, …, D. Gaver III. 1996. Modeling biofilm processes using the immersed boundary method. *J. Comput. Phys.* 129:57–73.